Journal of Hydraulic Structures
J. Hydraul. Struct., 2023; 9(1):1-17
DOI: 10.22055/jhs.2023.42950.1241

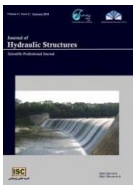

OPEN ACCESS

An investigation into the effects of tidal barrier operation on the tidal asymmetry in the Arvand Estuary

Mina Zakipour [1]
Farhad Yazdandoost [2]
Aref Farhangmehr [3]
Karim Alizad [2,4]

Abstract

The Arvand River forms the border between Iran and Iraq and is the only permanent river discharging into the Persian Gulf (PG). It is a tidal river adversely affected by sedimentation, which is more likely resulted from tidal asymmetry. The tidal barrier (TB) has remarkable effects on the tidal regime of the river. To assess the effects of a tidal barrier on the asymmetry of the tidal waves, it is critical to study the two main factors of closure percentage (CP) and closure duration (CD). This manuscript aims to investigate the tidal barrier effect on the asymmetry of the tidal waves propagating through the estuary. To evaluate tidal asymmetry, a Tidal Asymmetry Index (TAI) is introduced based on the relative phase angle of the M2 and M4 components through the river. A two-dimensional Delft3D hydrodynamic model is utilized. The tidal wave is flood dominant, and its relative phase angle increased slightly, from 90 to 135 degrees in Km 40 and then decreased to just under 90 degrees near the Abadan (65 km) and constant along the Abadan to Khorramshahr. The tidal barrier has changed the tidal regime in the river which leads to relatively constant tidal asymmetry during the 45km upward. To reach the highest TAI in the Arvand estuary, a closure percentage and duration of 55% and 180 minutes are estimated. The tidal barrier operation also adversely affects the amplitude of the M2 and M4 components. M4 component amplitude increases before reaching the TB and then decreases. The decrease is more elaborated from kilometer 45 onward. Increasing the closure percentage amplifies the changes described above, but it has little effect on the general trends.

Keywords: Arvand Estuary, Sediment, Tidal asymmetry, Tidal barrier, Persian Gulf.

Received: 02 February 2023; Accepted: 26 March 2023

[1] Department of Civil Engineering, K. N. Toosi University of Technology, Tehran, Iran. E-mail: minazakipour91@gmail.com (**Corresponding Author**).
[2] Department of Civil Engineering, K. N. Toosi University of Technology, Tehran, Iran.
[3] Institute of Geophysics, University of Tehran, Tehran, Iran.
[4] Belle W. Baruch Institute for Marine and Coastal Sciences, University of South Carolina, 209A Sumwalt Building, Columbia, SC 29208.

1. Introduction

Estuaries are economically and environmentally important due to factors such as shipping, tourism, ecology, and commercial fisheries [1]. Sediment transport plays a critical role in the dynamics of these systems [2, 3]. The amount of transported sediments depend on parameters such as flow regime, current speed and sediment texture [4, 5]. In the tidal zones, several processes that take place within a tidal cycle play an essential role in sediment transport [6-8]. Tidal asymmetry is one of the most effective phenomena in sediment transport over each tidal cycle [9-11], which affects the long-term erosion, transportation and sedimentation and associated large-scale morphological changes in the tidal estuaries [12-14]. This paper focuses on reducing tidal asymmetry using tidal barriers as an engineering solution to mitigate sedimentation in the Arvand Estuary.

Tidal asymmetry, as an essential phenomenon is caused by the distortion of the tidal wave [9-11, 15] due to channel friction, intertidal areas and marshes [10, 16] during propagating from the open sea into the tidal zone. The friction of the channel with more effect during the low water and friction of the intertidal zone and marshes during high-water slows down the water propagation.

Understanding the tidal asymmetrical behavior and variability [9, 10, 17] and the consequent effects on residual sediment transport and morphodynamics [18-20] are helpful in coastal area management [21-23]. The difference between durations of rising and falling phases due to tidal asymmetry leads to an offset between the velocities of flood and ebb tides. The higher flood velocity, transports a larger amount of sediment from the sea to the estuary compared to the sediment export from the estuary to the sea, while the ebb dominant condition flushes more sediment out through the estuary [24, 25].

A tidal barrier (TB) is a control gate that alters the tidal asymmetry [26-28]. The TB could be applied to completely block the river cross section, for a period of time around low water to accelerate the consolidation and sedimentation that cause to decrease the tidal volume. On the other hand, the TB structure could constrict the cross-section to reach a more symmetric tide[28]. In the flood-dominated fluvial estuaries, which are affected by a more significant amount of upstream sediment transport from the river due to higher flood flow than the ebb flow, the TB operation would reduce the upstream sediment transport, but the ebb current and downstream sediment would not be altered [29-32]. Hence, TB can be helpful in sediment transport management.

Extensive studies have been conducted on tidal asymmetry and its effect on sediment transport [30, 33]. In addition, the construction of TB has been considered an effective solution to reach more symmetric tide[33]. Arvand estuary, as one of the most important estuaries in Iran is facing problems such as erosion at the mouth of the estuary and sedimentation in the river bed. So far, the effects of tidal asymmetry in the sediment transport regime have not been investigated in this estuary. Hence, this research aims to assess the tidal asymmetry and the effect of its control by applying TB. In addition, the presented relations to evaluate the asymmetry are applicable in one cross-section. However, it is important to maintain tidal symmetric along the river. In this study, a new index is presented to evaluate the preservation of symmetry along the river to assess different scenarios.

2. Study area

The Arvand estuary is located in the southwest of Iran. This fluvial estuary receives flow and sediment from the Arvand River. Arvand River -also known as Shatt-al-Arab [34]- is one of the longest tidal rivers in the border of Iran-Iraq which is formed by the conjunction of the Tigris and Euphrates rivers in Iraq and Karun River in Iran (Figure 1-b) [35]. Three major cities, such as Abadan, Khoramshahr and Basra, are located around it (Figure 1-b), with the river running mainly towards the south to reach the Persian Gulf [36]. Before discharging into the Persian Gulf (Figure 1-c), the river varies from 270–2500 m in width and 9–15 m in depth, which implies that it is navigable. It supports marine habitats along the northwest coast of the Persian Gulf and in the Mesopotamian marshes [37].

The hydrodynamic of the estuary is affected by upstream discharge and downstream tides. The tide in the estuary is classified as semi-diurnal, with an average rise of 2.6 m at the mouth of the river near the Persian Gulf [34]. The tide affects the upstream river by an average of 1.4 m at Abadan city (about 74 km from the river mouth) and continues upstream [38, 39].

In recent decades, considerable dam construction, climate changes and reduction in rainfall amounts have reduced the riverine discharge, which resulted in the domination of tidal currents. Consequently, this river is adversely affected by the following effects:

- Increasing the salinity intrusion length [40, 41]
- Increasing the rate of sea sediments intrusion [42]
- Changes in tidal asymmetry in the river [42, 43]
- Tidal forcing leading to erosion of the river mouth [42], intensified by the above factors within a period of time.

The consequence of the above-mentioned items could be seen in the long-term changes in Arvand estuary. The results of tracking the changes of water body boundaries by satellite images were extracted from Global Surface Water Explorer (GSWE) datasets (https://global-surface-water.appspot.com/) [44]. GSWE uses the entire archive of the Landsat 5 TM (Thematic Mapper), the Landsat 7 ETM+ (Enhanced Thematic Mapper Plus), and the Landsat 8 OLI (Operational Land Imager) orthorectified, TOA (Top of Atmosphere) reflectance, and brightness temperature images acquired from March 16, 1984, until now [45]. In Figure 1-b, the green area used to be dry land, which has been gradually affected by tidal currents and changed from dry land to a tidal zone. However, the orange-colored area changed from an intertidal to an inundated region in recent years. In general, the river mouth is changing and deviating landward due to the erosion by the tidal currents, affecting tidal regime and asymmetry. On the other hand, the sea level rise can also lead to the aggravation of tidal asymmetry [46]. Resulting tidal asymmetry intensify the erosion process.

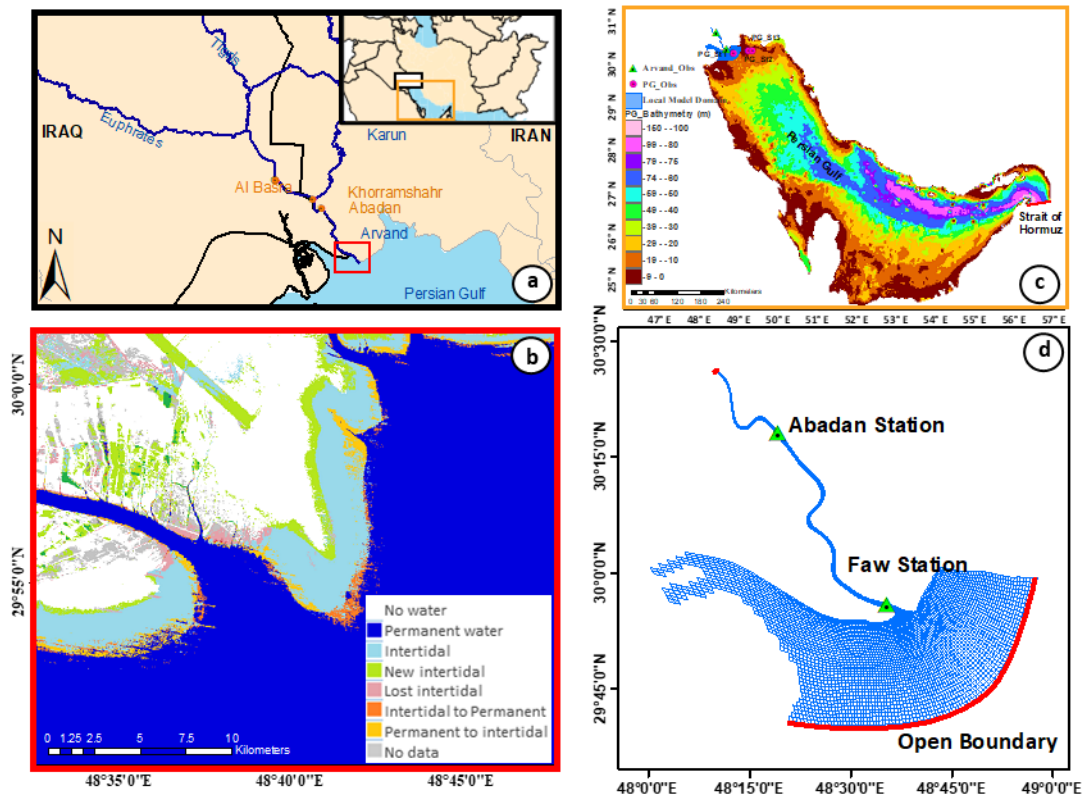

Figure 1- (a) Arvand estuary location in the Soutwest of Iran. (b) Long-term changes of Arvand estuary entrance adopted from Global Surface Water Explorer (GSWE), blue area: permanent water-covered area, sky blue: tidal zone, green: dry land converted to intertidal area, pink: intertidal area converted to dry lands, orange: intertidal area converted to permanent water covered, yellow: permanent water covered area converted to tidal zone, gray: area without data (c) PG bathymetry (GEBCO and Admiralty Charts), observational station, location of the PG model open boundary. (d) Delft3D curvilinear mesh of Arvand estuary model, observational stations along the estuary.

3. Methodology

To evaluate TB effects on tidal wave propagation, a 2D numerical model is developed and calibrated for upstream discharge and downstream tidal oscillations, disregarding the TB. Downstream tidal oscillations are extracted from a regional PG model. Afterward, different TB operation is assessed using parameters such as closure duration and closure percentage. Finally, to evaluate the functionality of TB, the symmetric condition is investigated.

3.1. Numerical modelling

The Delft3D model, developed by Delft Hydraulics (www.wldelft.nl) was operated to simulate the hydrodynamics of the study area. It is an integrated modeling suite that solves shallow water equations to simulate two-dimensional (in either the horizontal or a vertical plane) and three-dimensional flow, sediment transport and morphology, waves, water quality and ecology and is capable of handling the interactions between these processes (https://www.deltares.nl/en/software/delft3d-4-suite/). The Delft3D 2-DH model which utilizes shallow water equations were used. For the sake of conciseness, the demonstrations of the

equations are omitted. For a detailed description of the hydrodynamics and numerical scheme of Delft3D, see Lesser et al.[47] and Van der Wegen and Roelvink [48].

The regional PG model was limited to the Strait of Hormuz downstream and Arvand Estuary upstream. The surface elevation at the open boundary of the PG model at the Strait of Hormuz was predicted based on tidal constituents from Alosairi & Pokavanich, 2017. The curvilinear grid approach was incorporated to create a grid while allowing for relatively coarser grids in lower interest areas. The PG model contains 543000 elements with varying grid sizes from 1000 m in the deep area to 500 m in mid- depth and 200 m in the shallow water. The local model resolves the hydrodynamic from the seaward end of the Arvand estuary up to the Khorramshahr Port at approximately 80km distance from the PG.

The downstream boundary condition is extracted from regional model water level oscillations, and the upstream boundary condition was defined as river discharge at Khorramshahr boundary. The curvilinear mesh with 18000 elements captures the river section by dividing it into 20 segments with a length of about 100 to 150m (Figure 1-d).
Bathymetry data resources include the General Bathymetry Chart of the Oceans (GEBCO) on the 15 arc-second interval gridded data [49], Admiralty chart 2888 of the Strait of Hormuz and 3842, 3843, 3844 and 1235 for the Arvand river.

3.2. Tidal Barrier Operation Mode variants

The basic principle of the TB operation is to impede the flood wave to slow it down. This stretches out the time between high and low water levels, decreasing tidal asymmetry. The operation of TB, which is applied downstream of the Faw station location (Figure 1-d), starts at low water by reducing the river open section area by a certain percentage. The closure percentage varied between 15% and 85%. The closure percentage is defined for this context Equation 1 in which D_{open} is the existing water depth, and D_{closed} is the barrier opening height when the section is closed.

$$closure\ percentage = \left(1 - \frac{D_{closed}}{D_{open}}\right) \times 100\% \quad (1)$$

The closure duration is the other effective parameter, which refers to the time the TB is closed. After the closure duration has passed, the barrier will be opened again. The duration of the closure varies between 180 to 360 minutes. To determine the effects of closure duration, closure percentage, and discharge values on the TB operation, several simulations were conducted as below:

- To investigate different closure percentages (18%, 27%, 36%, 45%, 55%, 64%, 72%, 82%) effects, a constant discharge of 200 m^3/s as an annual average discharge of the river [50] and a closure duration of 5 hours,
- to investigate different closure duration (3, 4, 5 and 6 hours) effects, a constant discharge of 200 m^3/s and a closure percentage of 45%, and
- to investigate different discharge (200, 400 and 600 m^3/s) effects, a constant closure percentage of 45% and a closure duration of 5 hours are applied.

3.3. Evaluation criteria

3.3.1. Model results evaluation

To evaluate/validate how much the numerical model results are consistent with the observation data, the Kling-Gupta Efficiency (KGE) test is used here. The KGE equation (۲) is revised and enriched form of Nash-Sutcliffe Efficiency (NSE) [51]. It is a valuable tool for the similarity assessment of the simulation and observational data. KGE varies between -∞ to 1. When KGE is equal to 1, it indicates perfect simulation. As suggested by [52], the acceptable amount of this parameter was considered to be more than 0.6.

In equation (3), ED is the Euclidean distance between estimated and observed data. It is defined as a function of correlation (r), the ratio of the variance of the forecast to the variance of observation (α), and the ratio bias (β).

$$KGE = 1 - ED \quad (2)$$

$$ED = \sqrt{(r-1)^2 - (\alpha-1)^2 - (\beta-1)^2} \quad (3)$$

Furthermore, the Route Mean Square Error (RMSE) and correlation coefficients (CC) are calculated separately based on equations (4) and (5), where x, y and n denote the model variables such as water level and current speed in our case, observation variables, and the number of samples, respectively.

$$RMSE = \sqrt{\frac{1}{n}\sum\left(y_i - x_i\right)^2} \quad (4)$$

$$CC = \frac{\sum\left(x_i - \bar{x}\right)\left(y_i - \bar{y}\right)}{\sqrt{\sum\left(x_i - \bar{x}\right)^2 \sum\left(y_i - \bar{y}\right)^2}} \quad (5)$$

3.3.2. Tidal asymmetry evaluation

Tidal asymmetry is characterized based on the harmonic method. In this regard, amplitudes and phases of tidal constituents as tidal harmonics are resolved from simulated tidal data. Two or more tidal constituents with the frequency of ω which satisfies the relations $2\omega_1 = \omega_2$, $3\omega_1 = \omega_2$, and $\omega_1 + \omega_2 = \omega_3$ [53, 54] could interact and generate tidal asymmetry. Tidal asymmetry is quantified by two indicators included the amplitude ratios and the relative phase angle ($2\theta_1 - \theta_2$, $3\theta_1 - \theta_2$, and $\theta_1 + \theta_2 - \theta_3$) [10, 54], where, θ is the phase angle. These interactions are described in different references [55-57]. The distortion of the semi-diurnal tide can be represented as the non-linear growth of harmonic constituents with periods that are a fraction of the principal M2 tidal component. Since the M4 tidal component is the most important distorting tidal constituent, M2-M4 interactions have been widely recognized as the dominant tidal asymmetry components [10, 58].

In order to investigate the tidal asymmetry along the estuary, the new Tidal Asymmetry Index (TAI_{River}) is employed based on the relative phase between the M4 and M2 (Equation 6) and defined as Equation 7. This index indicates the bias of all sections along the river from the symmetric condition and varies between 0 to 1. The Closure TAI_{River} to 0, the higher symmetric condition is.

$$TA = 2\varphi_{M2} - \varphi_{M4} \quad (6)$$

$$TAI_{River} = \frac{1}{L}\int_{l:River\ Path}\left|\frac{TAI - 180}{180}\right| dl \quad (7)$$

4. Results and Discussion

The results are provided in two sections of numerical model calibration and validation of current condition and the results of applying different TB scenarios.

4.1. Numerical Model Calibration and validation

The calibration and validation of the hydrodynamic model were performed using data from the north of the Persian Gulf for the regional model and two stations along the river for the local model (Figure 1-c,d). The details of observational data incorporated for calibration and validation are shown in Table 1.

Table 1. Overview of the observational data for the model calibration and validation.

	Station name	Variable	Start Time	End Time
Regional model	PG_St1	Water Level	2017/08/09,00:00	2017/08/21,00:00
	PG_St2	Current speed	2017/08/03,00:00	2017/08/08,00:00
	PG_St3	Water Level	2019/06/03,00:00	2019/06/15,00:00
	PG_St3	Water Level	2000/09/23,00:00	2000/10/02,00:00
Local model	Abadan	Water Level/ Current speed	2015/10/16, 06:00	2015/10/16, 18:00
	Faw	Water Level/ Current speed	2015/10/16, 06:00	2015/10/16, 18:00

The regional model was calibrated against the bed roughness. After applying different constant roughness values and varying roughness values as a function of water depth, the best results were obtained for varying bed roughness coefficients in the range of 0.012-0.019 $s/m^{1/3}$. However, a constant bed roughness value of 0.015 $s/m^{1/3}$ is determined for the local model.

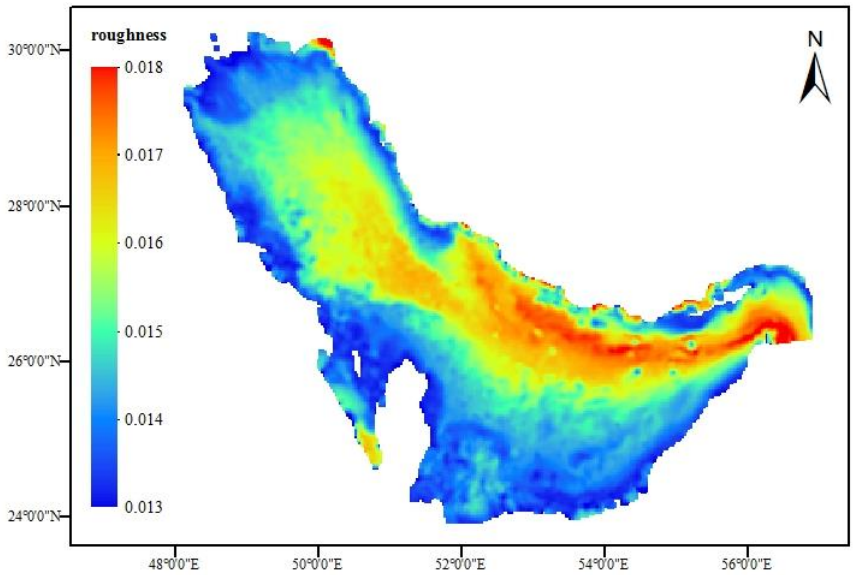

Figure 2. Varying bed roughness in PG model

The tidal wave propagates from the Strait of Hormuz and northwestward into the PG as a progressive wave. The model results show the semidiurnal tidal regime in the Arvand estuary. Comparisons between model results against the observational data in the regional and local models are shown in Figure 3 and Figure 4, respectively. Water level and current speed are in agreement with the selected gauge data. Table 2 lists the statistical parameters of the stations in the regional and local models. The CC values are more than 0.75, and KGE values are more than 0.73, therefore both regional and local models are suitably simulated

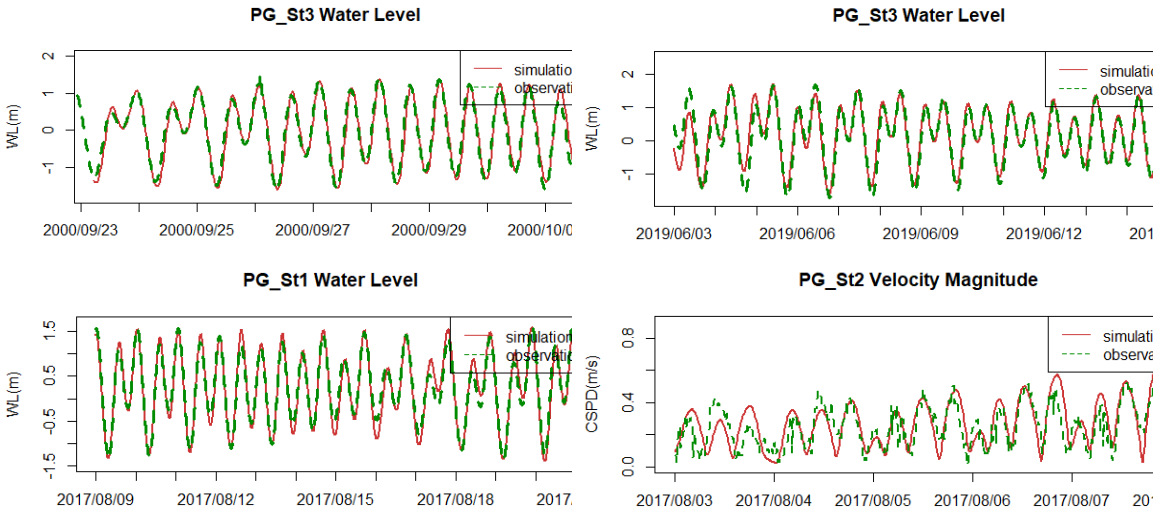

Figure 3. Regional model calibration and validation

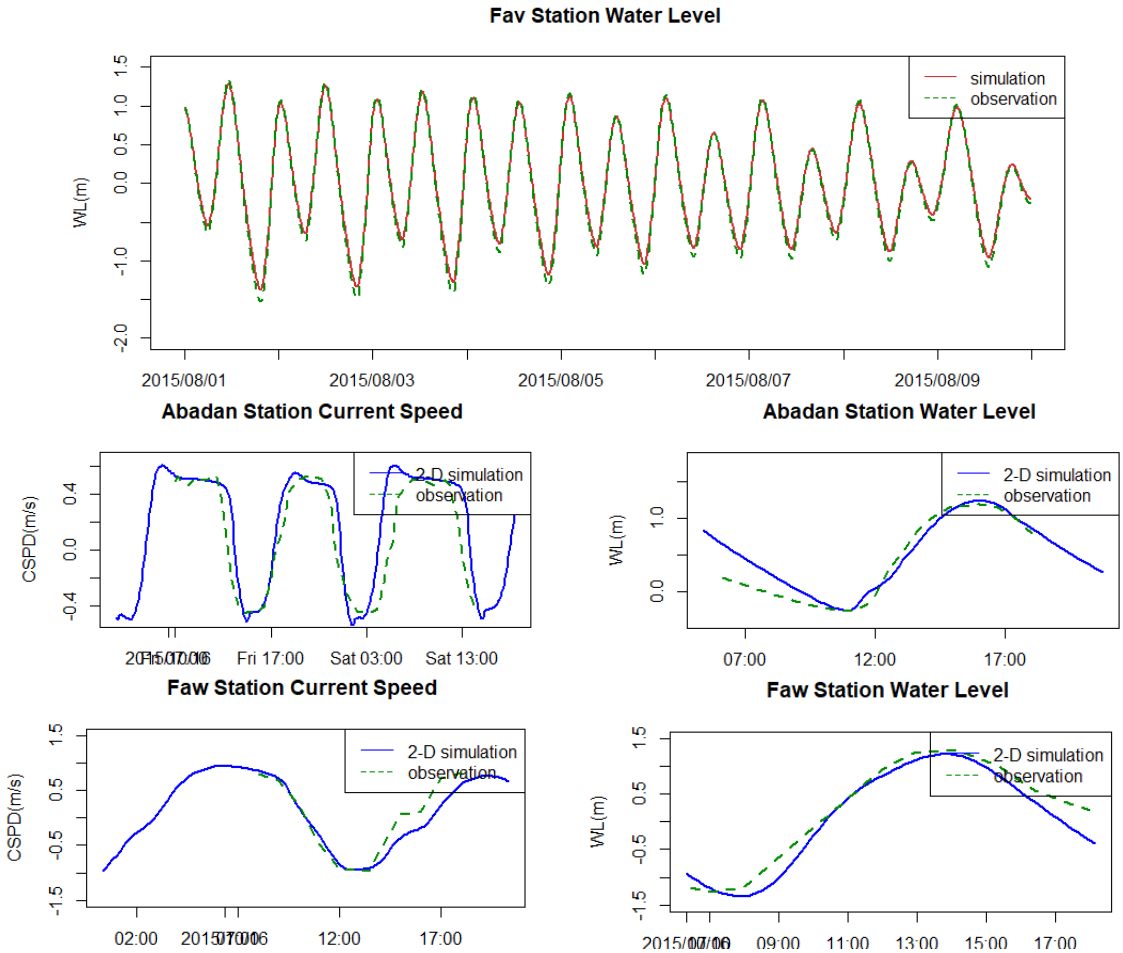

Figure 4. Local model calibration and validation

Table 2. Statistical parameters for the model calibration and validation.

	Station	Evaluated Variable	CC	RMSE	KGE
Regional Model	PG_St3_2000	Water Level	0.89	0.35 m	0.89
	PG_St3	Water Level	0.96	0.25 m	0.90
	PG_St1	Water Level	0.97	0.19 m	0.93
	PG_St2	Current speed	0.75	0.10 m/s	0.73
Local Model	Abadan	Water Level	0.96	0.19 m	0.95
	Abadan	Current speed	0.79	0.29 m/s	0.77
	Faw	Water Level	0.92	0.67 m	0.91
	Faw	Current speed	0.96	0.20 m/s	0.84

4.2. Tidal Barrier Simulation results and discussions

Tidal wave propagation along the Arvand estuary (from the northern part of PG to the upstream of Khorramshahr) has been assessed. In order to investigate the blockage range effects on TB operation, several closure percentages were modeled. A constant discharge of 200 m^3/s as an annual average river discharge [50] and a closure duration of 5 hours is applied.

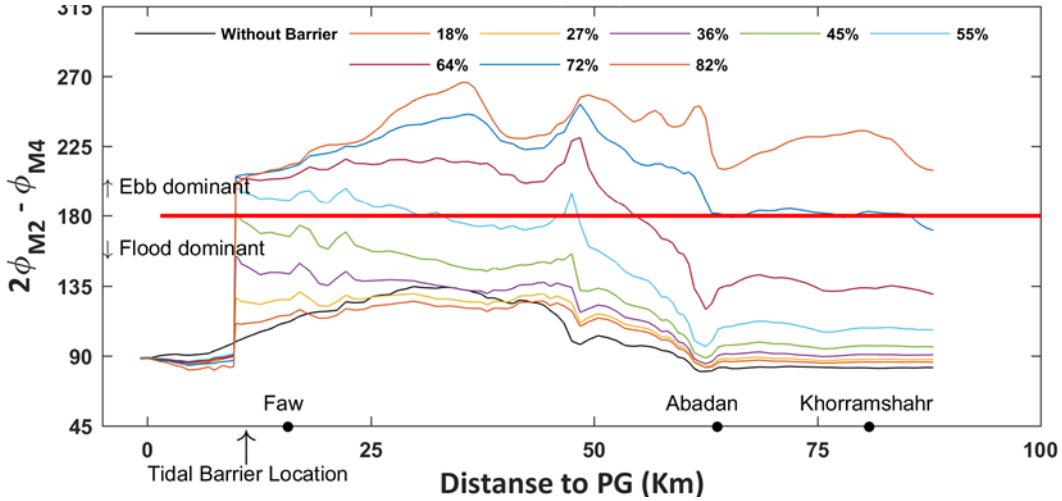

Figure 5. Tidal asymmetry along the river for different closure percentages (constant discharge:200m^3/s, closure duration: 5 hours)

In Figure 5 the bold red line represents the symmetric condition and border between ebb and flood dominant conditions based on the relative phase angle (2M2-M4), and the black line indicates the current condition asymmetry. The tidal wave is flood dominant, and its relative phase angle increased slightly, from 90 to 135 degrees in Km 40 and then decreased to just under 90 degrees near the Abadan (65 km) and constant along the Abadan to Khorramshahr. The results demonstrated reasonable correspondences with the asymmetry analysis by Lafta [59] regarding the flood dominant tidal regime and relative phase angle amounts near the estuary mouth.

The colored lines demonstrate the tidal asymmetry along the estuary by applying tidal barriers with different closure percentages (CP). Using the TB downstream of Faw station varied the asymmetry along the estuary and different behaviors were observed. For CP of 18% to 45%, the tidal wave pattern remains flood dominant along the estuary and follows a fairly similar pattern to the black line, particularly after Km 45, while CP of 55% and 64% experienced a mixed flood and ebb dominant tidal waves. In contrast, in CP above 72% the tidal wave patterns were ebb dominant. The results show the closure percentage of 55% met the most symmetric condition along the estuary to about 50 km from the PG.

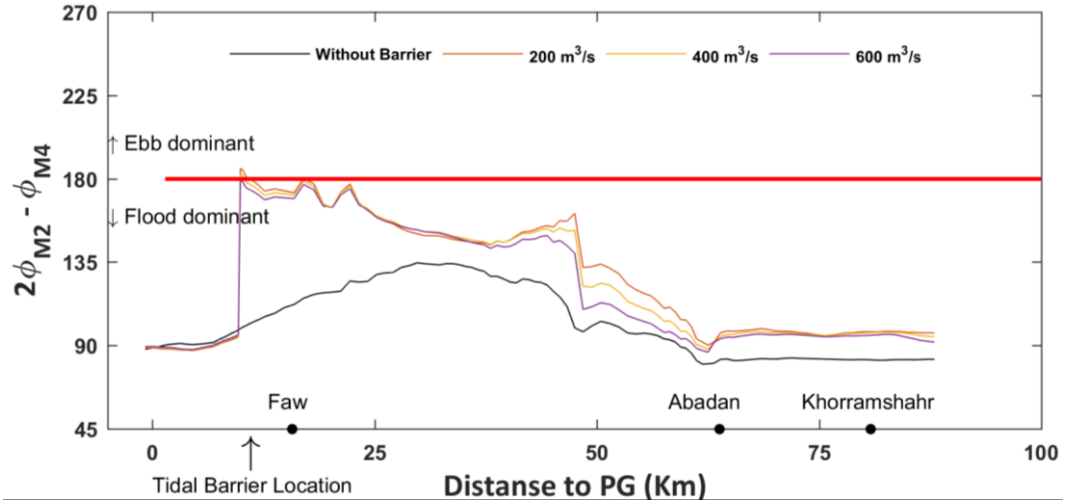

Figure 6. Tidal asymmetry along the river for different discharge values (closure percentage: 45%, closure duration: 6 hours)

In order to investigate different discharge effects on tidal asymmetry, TB with 45% CP and 5 hours CD with various discharges were simulated. Generally, changes in discharge values have no significant impact on tidal asymmetry. Increasing the flow rate values tends to make the observed pattern more like without a barrier condition. This behavior is more tangible in the middle of the estuary at Km of 45 to 65; however, less noticeable at the beginning and end of the estuary.

Hydrodynamic models with different TB closure duration and constant discharge of 200m^3/s, and closure percentages of 45% were assessed. The influence of closure duration is illustrated in Figure 7. The effect of the closure duration is not as effective as it was for the closure percentage along the river. There is a clear difference between different CDs in tidal asymmetry in the first 25 km off the entrance of the estuary. Additionally, various CD followed a similar decreasing trend after km of 25 with approximately equal asymmetry values. However, for CD shorter than 3 hours, the impact shows up to be minimal (negligible).

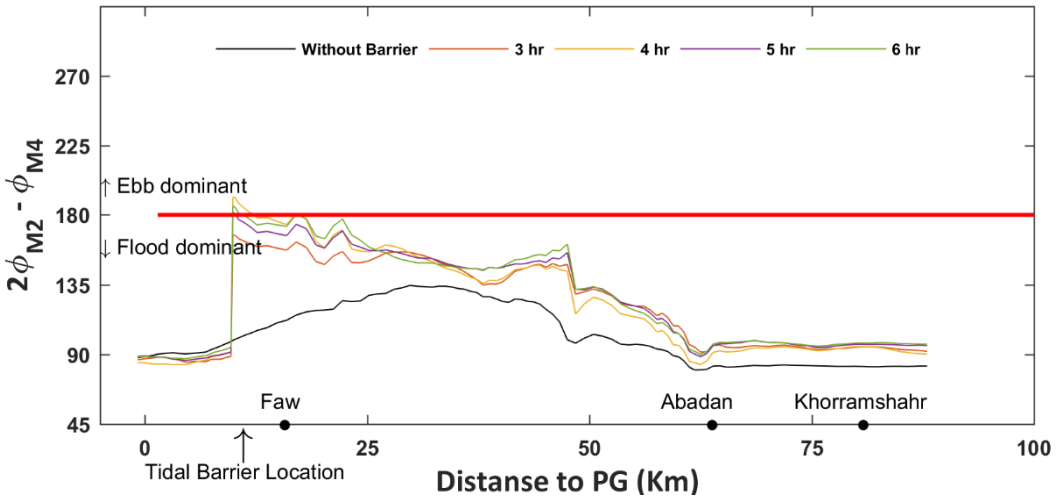

Figure 7. Tidal asymmetry along the river for different closure durations (closure percentage: 45%, discharge:200m^3/s)

Figure 8 demonstrates the effects of TB variations on tidal wave propagation process along the channel. Accordance reasonable correspondences with the Lafta [59] results in the Arvand estuary, in the current study the M4/M2 amplitude ratio is greater than 0.01, which shows the significant tidal distortion [60] in the tidal system. The amplitude of M2 component decreases upstream of the TB whereas this component has little changes before the TB. M4 component amplitude increases before reaching the TB and then falls. The decrease is more elaborated from kilometer 45 onward. Increasing the closure percentage amplifies the changes described above, but it has little effect on the general trends.

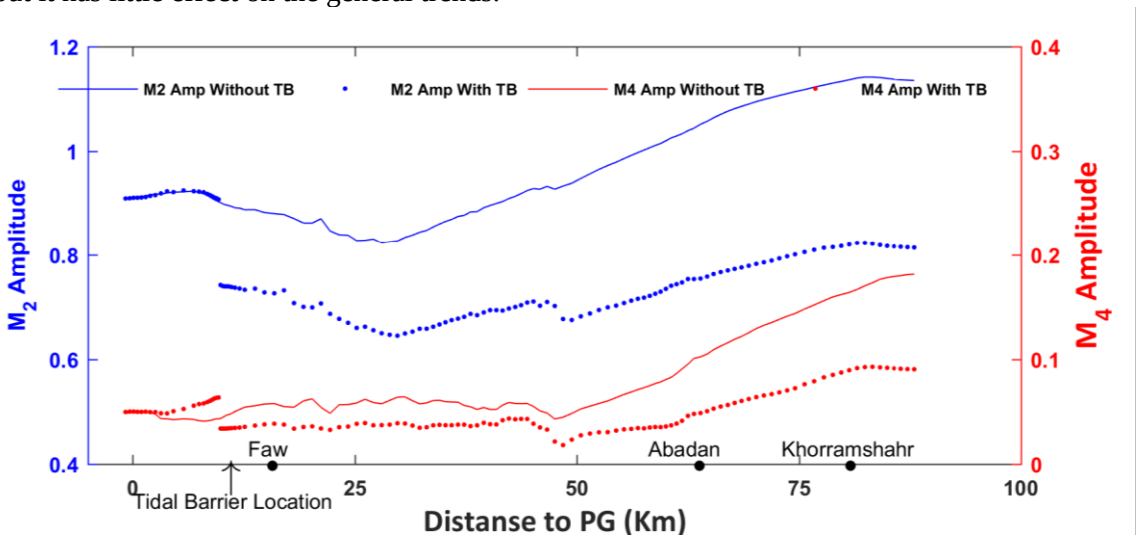

Figure 8. Variation of M2 and M4 tidal amplitude along the river by TB implementation

It is essential to maintain the continuity of symmetrical conditions along the river. The introduced TAI creates the opportunity to estimate continuity. It is calculated for different closure percentages and closure durations. Figure 9 shows TAI and M2 tidal amplitude immediately after TB (ζ) variation against different TB scenarios. In this figure, the circles' diameter represents the closure percentage magnitude, and various colors show the different closure durations. Implementing TB shows a decreasing rate of TAI before reaching the point where M2 tidal amplitude is about 0.7 and then increases.

According to the trend of TAI, it can be seen that for different CPs, when the CD is 3 hours, ζ has decreased to 0.5m. While, with the increase in CD, the decrease in ζ became more intense and reached less than 0.3 m in the condition of 6-hour blockage. The minimum value of TAI, which is equivalent to more symmetrical conditions, for 4 hours CD, is 0.12 for $\zeta = 0.72m$. When CD increased to 5 hours, the best symmetry occurred for $\zeta = 0.63m$ and TAI =0.05. After extending the CD to 6 hours, ζ increased to 0.69m and TAI to 0.1. To sum up, the 55% CP and 3hours CD with the minimum TAI has the most continuity of symmetry condition along the river.

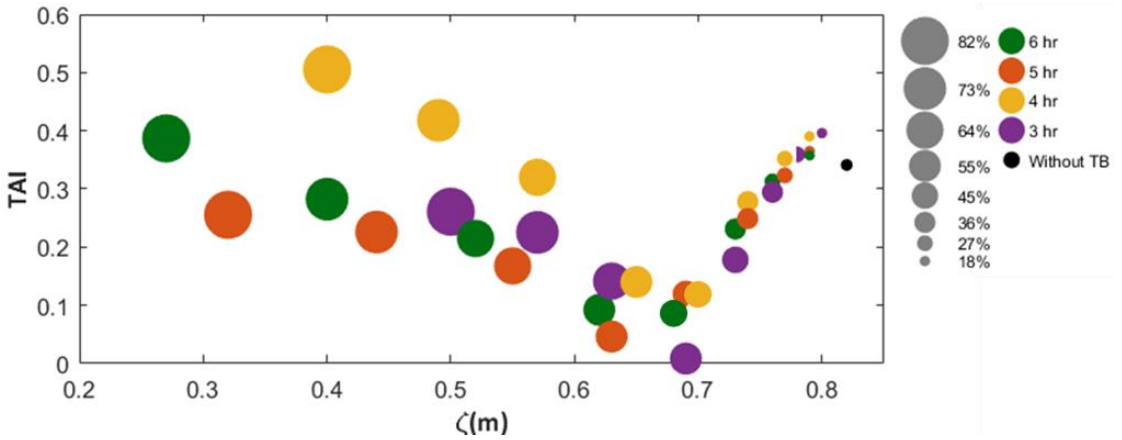

Figure 9. Tidal Asymmetry Index (TAI) for different tidal amplitude

5. Conclusion

Considering the importance of sediment transport in estuaries, in this research, tidal asymmetry as an effective component on the amount of sediment transport was investigated. The tidal asymmetry can be controlled using tidal barriers (TB) at the entrance of estuaries. In the current research, the tidal barrier effect on tidal symmetry was investigated in Arvand Estuary, which is located southwest of Iran and North of the Persian Gulf. In this regard, Closure duration (CD), Closure Percentage (CP) and river discharge were analyzed as variables affecting TB performance. Therefore, TBs with different CD, CP and riverine discharges were applied on a calibrated hydrodynamic model in the estuary. According to the results, a number of conclusions are summarized below:

The current condition is flood dominant, which is impressive with TB. Changes in the river discharge has a negligible effect on the barrier operation in the case study. Applying different closure duration has a binary impact on the TB operation in a way that its effects on the tidal asymmetry are inconsequential in the short duration (less than 3 hours). Additionally, increasing the closure duration to more than 3 hours has no significant difference on tidal asymmetry pattern. In contrast, various CPs have a significant effect on the tidal asymmetry patterns. For a constant river discharge and CD, increasing the CP from 18% to 82% leads to changes in the tidal asymmetry pattern from flood dominant to symmetric condition (in 55%) and then ebb dominant above 68%.

In addition, to examine the effect of TB on the relative phase angle, their effect on the amplitude of tidal components, which affects tidal asymmetry, was evaluated. Applying the TB decreases the amplitude of the M2 and M4 components landward. Also, it has an increased effect on the M4 seaward.

TAI was introduced in this paper as an index that measures the amount of continuity of symmetry along the estuary. In this work, the required length of the stretch of the estuary with a symmetric tide was not determined, so this index was evaluated for the whole length. According to the TAI results, the scenario with 55% CP and 3 hours CD is the one which provides the most symmetric stretch in the estuary. Real projects could apply this index to the required length.

References

1. Speirs, D.C. and W.S. Gurney, *Population persistence in rivers and estuaries.* Ecology, 2001. **82**(5): p. 1219-1237.
2. Teng, L., et al., *Lateral Variation of Tidal Mixing Asymmetry and Its Impact on the Longitudinal Sediment Transport in Turbidity Maximum Zone of Salt Wedge Estuary*. Journal of Marine Science and Engineering, 2022. **10**(7): p. 907.
3. Zhou, Z., et al., *Study of Sediment Transport in a Tidal Channel-Shoal System: Lateral Effects and Slack-Water Dynamics.* Journal of Geophysical Research: Oceans, 2021. **126**(3): p. e2020JC016334.
4. Teng, L., H. Cheng, and Y. Qiao. *Analysis of flow regime in the Turbidity Maximum Zone of Yangtze Estuary based on texture features of Tiangong-2 remote sensing images*. in *Proceedings of the Tiangong-2 Remote Sensing Application Conference*. 2019. Springer.
5. Kiaghadi, A., et al., *Longitudinal patterns in sediment type and quality during daily flow regimes and following natural hazards in an urban estuary: a Hurricane Harvey retrospective.* Environmental Science and Pollution Research, 2022. **29**(5): p. 7514-7531.
6. Chen, L., et al., *Lateral circulation and associated sediment transport in a convergent estuary*. Journal of Geophysical Research: Oceans, 2020. **125**(8): p. e2019JC015926.
7. Valizadeh, D. and M. Kolahdoozan. *Effect of Current Deflecting Wall on the Sedimentation in Tidal harbors*. in *ICHE 2010. Proceedings of the 9th International Conference on Hydro-Science & Engineering, August 2-5, 2010, Chennai, India*. 2010.
8. Van Rijn, L., *Tidal phenomena in the Scheldt Estuary.* Report, Deltares, 2010. **105**: p. 99.
9. Dronkers, J., *Tidal asymmetry and estuarine morphology.* Netherlands Journal of Sea Research, 1986. **20**(2-3): p. 117-131.
10. Friedrichs, C.T. and D.G. Aubrey, *Non-linear tidal distortion in shallow well-mixed estuaries: a synthesis.* Estuarine, Coastal and Shelf Science, 1988. **27**(5): p. 521-545.
11. Nidzieko, N.J., *Tidal asymmetry in estuaries with mixed semidiurnal/diurnal tides.* Journal of Geophysical Research: Oceans, 2010. **115**(C8).
12. Guo, L., et al., *Quantification of tidal asymmetry and its nonstationary variations.* Journal of Geophysical Research: Oceans, 2019. **124**(1): p. 773-787.
13. van Leussen, W., *Fine sediment transport under tidal action.* Geo-marine letters, 1991. **11**(3): p. 119-126.
14. Guo, L., et al., *A historical review of sediment export–import shift in the North Branch of Changjiang Estuary.* Earth Surface Processes and Landforms, 2022. **47**(1): p. 5-16.
15. Toublanc, F., et al., *Fortnightly tidal asymmetry inversions and perspectives on sediment dynamics in a macrotidal estuary (Charente, France).* Continental Shelf Research, 2015. **94**: p. 42-54.
16. Ridderinkhof, H., *Sediment transport in intertidal areas,* in *Intertidal Deposits*. 2019, CRC Press. p. 363-382.
17. Wang, Z., et al., *Tidal asymmetry and residual sediment transport in estuaries: a literature study and application to the Western Scheldt.* 1999.
18. Gatto, V.M., B.C. van Prooijen, and Z.B. Wang, *Net sediment transport in tidal basins: quantifying the tidal barotropic mechanisms in a unified framework.* Ocean Dynamics, 2017. **67**(11): p. 1385-1406.
19. Guo, L., et al., *Exploring the impacts of multiple tidal constituents and varying river flow on long-term, large-scale estuarine morphodynamics by means of a 1-D model.* Journal of Geophysical Research: Earth Surface, 2016. **121**(5): p. 1000-1022.

20. Postma, H., *Tidal flat areas*, in *Coastal-offshore ecosystem interactions*. 1988, Springer. p. 102-121.
21. Godin, G., *Frictional effects in river tides.* Tidal hydrodynamics, 1991. **379**: p. 402.
22. Guo, L., et al., *The role of river flow and tidal asymmetry on 1-D estuarine morphodynamics.* Journal of Geophysical Research: Earth Surface, 2014. **119**(11): p. 2315-2334.
23. Guo, L., et al., *River-tide dynamics: Exploration of nonstationary and nonlinear tidal behavior in the Y angtze R iver estuary.* Journal of Geophysical Research: Oceans, 2015. **120**(5): p. 3499-3521.
24. Winterwerp, J.C., *Fine sediment transport by tidal asymmetry in the high-concentrated Ems River: indications for a regime shift in response to channel deepening.* Ocean Dynamics, 2011. **61**(2): p. 203-215.
25. Wang, Z.B., et al., *Morphology and asymmetry of the vertical tide in the Westerschelde estuary*. Continental Shelf Research, 2002. **22**(17): p. 2599-2609.
26. Dissanayake, D., J. Roelvink, and M. Van der Wegen, *Modelled channel patterns in a schematized tidal inlet.* Coastal Engineering, 2009. **56**(11-12): p. 1069-1083.
27. Vos, T., *Tidal control in the Lower Ems: An indicative study into the effects of controlled barrier operation on the tidal asymmetry in the Lower Ems river*. 2021.
28. Oberrecht, D. and A. Wurpts, *Impact of controlled tidal barrier operation on tidal dynamics in the Ems estuary.* Die Küste, 81 Modelling, 2014(81): p. 427-433.
29. Chernetsky, A.S., H.M. Schuttelaars, and S.A. Talke, *The effect of tidal asymmetry and temporal settling lag on sediment trapping in tidal estuaries.* Ocean Dynamics, 2010. **60**(5): p. 1219-1241.
30. Kuang, C., et al., *Morphological process of a restored estuary downstream of a tidal barrier*. Ocean & Coastal Management, 2017. **138**: p. 111-123.
31. Lee, S. and J.L. Lee, *Estimation of background erosion rate at Janghang Beach due to the construction of Geum estuary tidal barrier in Korea.* Journal of Marine Science and Engineering, 2020. **8**(8): p. 551.
32. Eelkema, M., et al., *Morphological effects of the Eastern Scheldt storm surge barrier on the ebb-tidal delta.* Coastal Engineering Journal, 2013. **55**(3): p. 1350010-1-1350010-26.
33. Herrling, G., et al., *The effect of asymmetric dune roughness on tidal asymmetry in the Weser estuary*. Earth Surface Processes and Landforms, 2021. **46**(11): p. 2211-2228.
34. Haghighi, A.T., et al., *The impact of river regulation in the Tigris and Euphrates on the Arvandroud Estuary*. Progress in Physical Geography: Earth and Environment, 2020. **44**(6): p. 948-970.
35. Hajiabadi, A., S. Sakhdari, and R. Barati, *Study of morphologic changes in the past and predicting future changes of border rivers (case study: Arvand River, Iran-Iraq Border Line)*, in *Current Directions in Water Scarcity Research*. 2022, Elsevier. p. 153-163.
36. Etemad-Shahidi, A., et al., *Investigation of hydraulics transport time scales within the Arvand River estuary, Iran.* Hydrological Processes, 2014. **28**(25): p. 6006-6015.
37. UN-ESCWA and BGR, *Inventory of Shared Water Resources in Western Asia*. 2013, UN-ESCWA, BGR Beirut.
38. Etemad Shahidi, A., A. Saburi, and J. Parsa, *Control of salinity intrusion in Arvand estuary under different hydrological conditions.* Iran-water resources research, 2011. **7**(2): p. 50-60.

39. Zahed, F., A. Etemad-Shahidi, and E. Jabbari, *Modeling of salinity intrusion under different hydrological conditions in the Arvand River Estuary.* Canadian Journal of Civil Engineering, 2008. **35**(12): p. 1476-1480.
40. Etemad-Shahidi, A., J. Parsa, and M. Hajiani. *Salinity intrusion length: comparison of different approaches*. in *Proceedings of the Institution of Civil Engineers-Maritime Engineering*. 2011. Thomas Telford Ltd.
41. Etemad-Shahidi, A., et al., *Effects of sea level rise on the salinity of Bahmanshir estuary.* International journal of environmental science and technology, 2015. **12**(10): p. 3329-3340.
42. Passeri, D.L., et al., *The dynamic effects of sea level rise on low-gradient coastal landscapes: A review.* Earth's Future, 2015. **3**(6): p. 159-181.
43. Khojasteh, D., et al., *Sea level rise will change estuarine tidal energy: A review.* Renewable and Sustainable Energy Reviews, 2022. **156**: p. 111855.
44. Pekel, J.-F., et al., *High-resolution mapping of global surface water and its long-term changes.* Nature, 2016. **540**(7633): p. 418-422.
45. Hakimdavar, R., et al., *Monitoring water-related ecosystems with earth observation data in support of Sustainable Development Goal (SDG) 6 reporting.* Remote Sensing, 2020. **12**(10): p. 1634.
46. Jiang, L., et al., *Effects of sea-level rise on tides and sediment dynamics in a Dutch tidal bay.* Ocean Science, 2020. **16**(2): p. 307-321.
47. Lesser, G.R., et al., *Development and validation of a three-dimensional morphological model.* Coastal engineering, 2004. **51**(8-9): p. 883-915.
48. Van der Wegen, M. and J. Roelvink, *Long-term morphodynamic evolution of a tidal embayment using a two-dimensional, process-based model.* Journal of Geophysical Research: Oceans, 2008. **113**(C3).
49. Weatherall, P., et al., *A new digital bathymetric model of the world's oceans.* Earth and space Science, 2015. **2**(8): p. 331-345.
50. Alosairi, Y. and T. Pokavanich, *Seasonal circulation assessments of the northern Arabian/Persian Gulf.* Marine pollution bulletin, 2017. **116**(1-2): p. 270-290.
51. Gupta, H.V., et al., *Decomposition of the mean squared error and NSE performance criteria: Implications for improving hydrological modelling.* Journal of hydrology, 2009. **377**(1-2): p. 80-91.
52. Khajehei, S. and H. Moradkhani, *Towards an improved ensemble precipitation forecast: A probabilistic post-processing approach.* Journal of Hydrology, 2017. **546**: p. 476-489.
53. Guo, W., et al., *Contributions of different tidal interactions to fortnightly variation in tidal duration asymmetry.* Journal of Geophysical Research: Oceans, 2016. **121**(8): p. 5980-5994.
54. Song, D., et al., *Modeling studies of the far-field effects of tidal flat reclamation on tidal dynamics in the East China Seas.* Estuarine, Coastal and Shelf Science, 2013. **133**: p. 147-160.
55. Jewell, S.A., D.J. Walker, and A.B. Fortunato, *Tidal asymmetry in a coastal lagoon subject to a mixed tidal regime.* Geomorphology, 2012. **138**(1): p. 171-180.
56. Blanton, J.O., G. Lin, and S.A. Elston, *Tidal current asymmetry in shallow estuaries and tidal creeks.* Continental Shelf Research, 2002. **22**(11-13): p. 1731-1743.
57. Van de Kreeke, J. and K. Robaczewska, *Tide-induced residual transport of coarse sediment; application to the Ems estuary.* Netherlands Journal of Sea Research, 1993. **31**(3): p. 209-220.

58. Speer, P.E., D.G. Aubrey, and C.T. Friedrichs, *Nonlinear hydrodynamics of shallow tidal inlet/bay systems.* Tidal hydrodynamics, 1991. **321**: p. 339.
59. Lafta, A.A., *Investigation of tidal asymmetry in the Shatt Al-Arab river estuary, Northwest of Arabian Gulf.* Oceanologia, 2022. **64**(2): p. 376-386.
60. Lu, S., et al., *Propagation of tidal waves up in Y angtze E stuary during the dry season.* Journal of Geophysical Research: Oceans, 2015. **120**(9): p. 6445-6473.